Lithium Vapor Chemistry of Hyper-Stoichiometric Lithium Metatitanate $Li_{2.12(2)}TiO_{3+y}$

Keisuke Mukai,[a,c*] Masaru Yasumoto,[b] and Takayuki Terai[c]

[a] Institute of Advanced Energy, Kyoto University, Gokasho, Uji, 611-0011, Japan.

[b] Laboratory for Environmental Research at Mount Fuji, NPO Mount Fuji Research Station, 1-6-9 kojimachi, Chiyodaku, Tokyo 102-0083, Japan

[c] School of Engineering, The University of Tokyo, 7-3-1 Hongo, Bunkyo-ku, Tokyo 113-8656, Japan

* Corresponding author: k-mukai@iae.kyoto-u.ac.jp

Supporting Information Placeholder

Abstract

Developing a better ceramic breeder (Li-containing oxide) is a key challenge for realizing fuel-self-sufficient fusion reactors. Ceramic breeder pebbles of hyper-stoichiometric lithium metatitanate, $Li_{2+x}TiO_{3+y}$ (Li/Ti > 2), have been developed for a demonstration fusion reactor as high Li density enhances fuel tritium production. Previous studies have reported that Li loss by vaporization at high temperatures was largely enhanced by the increase in Li/Ti ratio and environmental moisture concentration. Minimizing the Li loss is a key issue for sufficient tritium breeding and reduced corrosion of structural steel. However, a suitable environmental parameter for hyper-stoichiometric $Li_{2+x}TiO_{3+y}$ pebbles has not yet been determined because of unavailability of thermodynamic data. Herein, a solid/gas equilibria for $Li_{2.12(2)}TiO_{3+y}$ was investigated by measuring vapor pressures using atmosphere controllable Knudsen cell high temperature mass spectrometry. The enhanced thermodynamic activities of Li and Li_2O in $Li_{2.12(2)}TiO_{3+y}$ in comparison with those in stoichiometric Li_2TiO_3 were obtained as functions of temperature and oxygen concentration. The equilibrium constants were used to achieve the optimum moisture concentration that can suppress the vapor reactions in a cylindrical breeding zone with inhomogeneous temperature distribution.

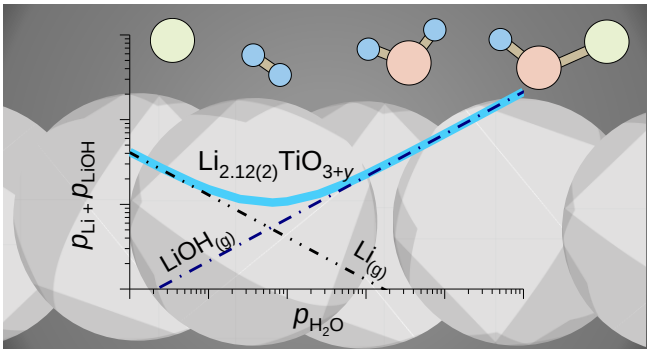

1. Introduction

Nuclear fusion is a promising source of sustainable and low-carbon energy using fuel of hydrogen isotopes. In a deuterium–tritium (DT) fusion reactor, ceramic breeder converts kinetic energy of neutrons into heat and produces fuel tritium through transmutation of Li (i.e., $^{6}Li + {}^{1}n \rightarrow {}^{3}T + {}^{4}He$). To maintain fuel-self-sufficiency, amount of tritium recovery from the blanket must be greater than that of tritium consumption in the DT plasma.[1] Ceramic breeder pebbles packed in the blanket are exposed to a high flux of 14 MeV neutrons at high temperatures for years of reactor operation. Release of bred tritium from the breeder pebbles is enhanced by adding 0.1 vol.% of H_2 into helium sweep gas.

Presently, ternary oxides of lithium metatitanate (Li_2TiO_3) and lithium orthosilicate (Li_4SiO_4) are selected as the reference ceramic breeder materials for the ITER test blanket module.[2–5] For a demonstration fusion reactor, advanced ceramic breeders have been developed in order to improve mechanical properties[6] and reduce activation.[7] Hyper-stoichiometric lithium metatitanate $Li_{2+x}TiO_{3+y}$ (Li/Ti > 2) is an advanced breeder material with a higher content of Li than stoichiometric Li_2TiO_3, which enhances tritium production.[8] $Li_{2+x}TiO_{3+y}$ is known to have a resistance to reduction of Ti ($Ti^{4+} \rightarrow Ti^{3+}$) at high temperatures which forms oxygen defect.[9] β-Li_2TiO_3 has a monoclinic $C2/c$ structure with an ordered stacking of Li–O and Li–Ti–O layers where the cations occupy the octahedral sites.[10,11] It is known that monoclinic β-Li_2TiO_3 forms a solid solution in the TiO_2 range of 47–51 mol%.[12] In the monoclinic crystal, excess Li is mainly accommodated by cation displacement and interstitial Li in a reducing atmosphere as predicted by the molecular dynamics and first principles calculations.[13–15] The existence of interstitial Li atom at tetrahedral site in the Li–O layer is experimentally shown by neutron diffraction.[16]

In previous experiments, altered chemical properties of $Li_{2+x}TiO_{3+y}$ from Li_2TiO_3 have been reported, including faster tritium diffusion,[17] enhanced grain growth during heating,[18] and higher affinity for moisture and carbon dioxide.[19] It is noteworthy that mass loss by evaporation of Li-containing species at high temperatures were enhanced by the increase of Li/Ti ratio.[20,21] The Li loss by evaporation should be minimized for sufficient breeding of tritium fuel during reactor operation. Additionally, the vaporization behavior affects chemical compatibility between ceramic breeder and reduced-activation ferritic/martensitic (RAFM) steels; the Li-containing gaseous species are corrosive and form a double oxide layer on surface of the RAFM steels,[22–25] in which the growth is controlled by oxygen diffusion in the layers.[23] The Li mass loss and corrosion were critically enhanced by the increases in moisture

concentrations.[20,26] The corrosion of the RAFM structural steel by $Li_{2.17}TiO_{3+y}$ was reported to be more severe than that by Li_2TiO_3, but less severe than that by Li_2O.[27]

Despite the importance of controlling the vaporization of Li-containing species in a breeding blanket, an optimum condition for suppressing the Li loss has not yet been determined until today. For such analysis, thermodynamic data of $Li_{2+x}TiO_{3+y}$ is needed in addition to mass transfer studies, because vaporization behavior can largely vary depending on environmental parameters such as moisture concentrations. Therefore, the present study aims to evaluate thermodynamic properties of hyper-stoichiometric lithium metatitanate and to determine optimum blanket conditions by using the experimental data. Atmosphere controllable Knudcen cell mass spectroscopy was employed to measure equilibrium gas pressures over ceramic breeder pebbles under vacuum/reducing conditions.

2. Experimental Method

2.1. Samples preparation.

Stoichiometric and hyper-stoichiometric lithium metatitanate pebbles with natural isotope abundance were supplied from National Institutes for Quantum and Radiological Science and Technology. Figure 1 shows electron microscope images of the pebbles. The stoichiometric Li_2TiO_3 pebbles were fabricated by sol-gel method by sintering at 1373 K under air atmosphere (Figure 1a).[18] The stoichiometric pebbles had an average pebble diameter of 1.0 mm, sintering density of 84.1% T.D., and grain size of <5 μm. The hyper-stoichiometric pebbles were fabricated by emulsion method by sintering at 1373 K under N_2 atmosphere.[18] Average pebble diameter and sintering density of the hyper-stoichiometric pebbles were 1.33 mm and 87.6% T.D., with grain sizes smaller than 10 μm (Figure 1b). By powder X-ray diffraction using Cu–*K*α (RINT-2500, Rigaku), it was confirmed that these pebbles had no diffraction peak from impurity phase such as $Li_4Ti_5O_{12}$, Li_4TiO_4 or Li_2CO_3. By inductively coupled plasma optical emission spectrometer (ICP-OES), chemical compositions of the stoichiometric and hyper-stoichiometric pebbles were analyzed to be Li/Ti = 2.00(2) and 2.12(2), respectively. In this study, chemical compositions of the stoichiometric and hyper-stoichiometric samples are written as Li_2TiO_3 and $Li_{2.12(2)}TiO_{3+y}$. Noted that the hyper-stoichiometric composition does not mean that excess amount of oxygen is accommodated in Li_2TiO_3; the charge neutrality is maintained by interstitial Li, displacement of cations, and electrons, while interstitial oxygen is unfavorable according to the computational results.[14,15]

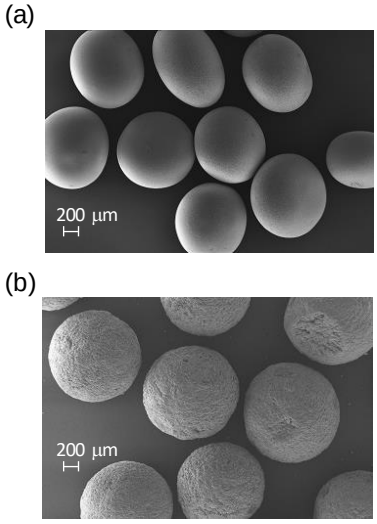

Figure 1. Scanning electron microscope images of (a) the stoichiometric Li_2TiO_3 and (b) the hyper-stoichiometric $Li_{2.12(2)}TiO_{3+y}$ pebbles.

2.2. Knudsen cell mass spectrometer

Figure 2 shows the schematic representation of the Knudsen cell mass spectrometer. The pebbles were packed in a Pt crucible. The crucible was placed in a Pt Knudsen cell with an orifice diameter of 0.5 mmφ. Molecular beams of gas species from the orifice were positively ionized by accelerated electrons. Using an analyzing magnet, ions with specific mass numbers were selectively detected by a secondary electron multiplier. Measurements under the condition of simulated sweep gas was carried out by introducing D_2 gas from the inlet tube.[28] ^{7}Li isotope was analyzed for all of Li-containing vapor species. All of the measurements were carried out with the ionization voltage of 30 V. The voltage was enough high to obtain ion intensities of the vapor species that appeared in the experiments, at which no fragmentation was observed (Figure S1 in Supporting Information (SI)). Ion intensity of ion species i, I_i, was obtained by subtracting the count rate with closed shutter from the one with opened shutter. Then I_i was converted into the corresponding partial pressure p_i (Pa) by the following equation:

$$p_i = \frac{k_m I_i T}{\sigma_i \gamma_i n_i} \quad (1)$$

where T is the temperature of sample (K), k_m is the apparatus constant, σ_i is the relative ionization cross section, γ_i is the gain of the secondary electron multiplier, and n_i is the isotopic abundance ratio. Isotopic abundance ratio of ^{7}Li

was set to be 92.5%. Atomic ionization cross sections were taken from Mann,[29] while those of molecules were calculated by the method proposed by Kordis and Gingerich.[30] Before measurement, all pebble specimens were heated at 873 K for 8 h in the Knudsen cell to avoid possible effects of absorbed water and carbon dioxide.

Thermodynamic activity in a mixture a_i is given by the following equation:

$$a_i = p_{i,\text{mixture}}/p_{i,\text{pure}} \quad (2)$$

where $p_{i,\text{mixture}}$ and $p_{i,\text{pure}}$ are the vapor pressures of species i from the mixture and the substance, respectively. Given that the thermodynamic activity of the pure substance in a condensed phase equals to unity, reaction enthalpy at the standard temperature ΔH_{298} is calculated by the third low treatment as follows:

$$\Delta H_{298} = -(\Delta fef - R\ln K)T \quad (3)$$

where *fef* is the free energy function, R is the universal gas constant, and K is the equilibrium constant. The *fef* data of $D_{2(g)}$, $D_2O_{(g)}$, $Li_{(g)}$, $O_{2(g)}$, $Li_2O_{(s)}$, $Li_2TiO_{3(s)}$, and $TiO_{2(s)}$ were taken from the JANAF table.[31] As no *fef* data of $LiOD_{(g)}$ was available on the database, that of $LiOH_{(g)}$ was employed alternatively.

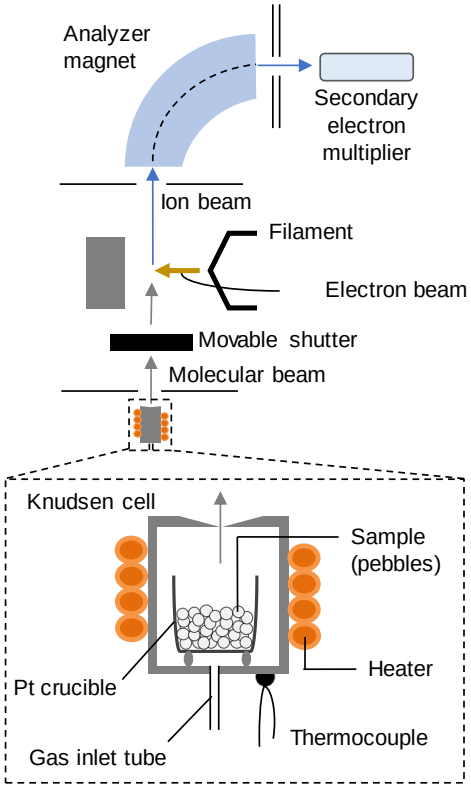

Figure 2. Schematic representation of the Knudsen cell mass spectrometer.

2.3. Calibrations

With a metallic Ag standard sample, T was calibrated with the temperature measured by a thermocouple T_m. The vapor pressure of $Ag_{(g)}$ from the Ag metal was measured in the temperature range from 1113 K to 1323 K (heating up in 10 K increments). Thereafter, the measurements during cooling were carried out from 1323 K to 1148 K in 25 K decrements. The pressures of $Ag_{(g)}$ increased exponentially with the inverse of T_m during heating as shown in Figure S1 in the Supporting Information (SI). At T_m = 1253 K, a drop in pressure was observed. The change in the trend was observed in the data during heating above the temperature. Thus, this drop indicates the decrease in Ag activity ($a_{Ag,\ alloy}$ <1) caused by the melting of the Ag metal and the subsequent formation of Ag–Pt alloy. With the known melting point of the Ag metal (1234.95 K), T_m was calibrated to the temperature of sample T. The apparatus constant k_m was once obtained by comparing the values of $p_{Ag,metal}$ (T < 1235) with the reported pressures of $Ag_{(g)}$ from the Ag metal by Alcock *et al.*[32] To avoid possible variation of k_m in each run, k_m was calibrated with Ar standard gas filled in the Knudsen cell. A specific amount of Ar gas was introduced in the Knudsen cell and then measured.–

3. Results and Discussion

3.1. Vapor pressure measurements

Equilibrium gas pressures from the pebbles were measured under the vacuum condition and, thereafter, in a reducing atmosphere by introducing D_2 gas. The measurements were performed from a lower to higher temperature. Figure 3 and Figure 4 show the vapor pressures measured in vacuum and D_2 atmospheres, respectively. Under the vacuum condition, Li gas was detected above 1155 K, at which gaseous phases of Li, LiO, Li_2O, and O_2 were observed. In D_2 atmosphere, gaseous phases of Li, LiOD, D_2, and D_2O were measured, in which the partial pressure of oxygen gas was below the detection limit of ~10^{-5} Pa. The measured partial pressures of $LiO_{(g)}$ (mass number: 23) from Li_2TiO_3 was even higher than $Li_{(g)}$ in contradiction to the previous measurement for Li_2TiO_3, in which p_{Li} is approximately three order of magnitude higher than p_{LiO}.[33] The high ion intensity of mass 23 may be caused by ^{23}Na impurity in the pebbles mixed during the pebble fabrication. By ICP-OES, the concentration of ^{23}Na impurity in the Li_2TiO_3 pebbles was analyzed to be 630 ppm. Background ion counts of O_2 and D_2 measured while closing the movable shutter were higher than the other gas species, resulting in relatively large errors in p_{D_2} and p_{O_2} by error propagation. In the measurements, the vapor pressures were slightly influenced at 1428 K ($10^4/T$ = 7.0 K^{-1}) by the monoclinic-cubic (β-γ) transformation, which is reported to occur at 1423 K.[12] A non-contiguous Li pressure from

the hyper-stoichiometric pebbles at $1350 < T < 1400$ K may be explained by two-step phase transformation in the Li-rich regime,[12] namely $\beta \rightarrow \beta + \gamma \rightarrow \gamma$. From the measured gaseous species, the vapor reactions in vacuum atmosphere were assumed as follows.

$$Li_2TiO_{3(s)} \leftrightarrow 2Li_{(g)} + 0.5O_{2(g)} + TiO_{2(s)} \quad (4)$$

$$Li_{2+2x}TiO_{3+x(s)} \leftrightarrow 2Li_{(g)} + 0.5O_{2(g)} + xLi_2O_{(s)} + TiO_{2(s)} \quad (5)$$

In D_2 atmosphere, the following reactions were considered.

$$Li_2TiO_{3(s)} + D_2O_{(g)} \leftrightarrow 2LiOD_{(g)} + TiO_{2(s)} \quad (6)$$

$$Li_{2+2x}TiO_{3+x(s)} + D_2O_{(g)} \leftrightarrow 2LiOD_{(g)} + xLi_2O_{(s)} + TiO_{2(s)} \quad (7)$$

$$D_{2(g)} + 0.5O_{2(g)} \leftrightarrow D_2O_{(g)} \quad (8)$$

After the measurement, X-ray diffraction was performed on the pebbles. The diffraction patterns showed no peak from impurity phase, which indicates formation of non-stoichometric phase. But, we simply assumed formation of TiO_2 instead of the hypo-stoichiometric phase because the ratio of $Li_{(g)}$ and $O_{2(g)}$ remains 4:1 even with product of $Li_{2-2x}TiO_{3-x}$. The temperature dependencies of the vapor pressures in vacuum and D_2 atmosphere are listed in Table S1 and S2 in SI, respectively. Reliability of the observed pressures was confirmed by calculating reaction enthalpies by the third low treatment. For the measurements under vacuum and D_2 atmospheres, the following two gas reactions were considered:

$$Li_2O_{(g)} \leftrightarrow 2Li_{(g)} + 0.5O_{2(g)} \quad (9)$$

$$LiOD_{(g)} + 0.5D_{2(g)} \leftrightarrow Li_{(g)} + D_2O_{(g)} \quad (10)$$

The reaction enthalpies in Eq. (9) from the stoichiometric and hyper-stoichiometric samples were evaluated to be 477.8 ± 5.8 and 491.7 ± 10.1 kJ/mol respectively. It is noted that the enthalpies and error denote average value and standard deviation of the data at each temperature to allow a direct comparison with previous data.[34] The obtained values agreed with the previous experimental value (481.8 ± 11.2 kJ/mol)[34] and the data from the MALT database (491.4 kJ/mol).[35] The reaction enthalpies of eq. (10) from the stoichiometric and hyper-stoichiometric samples were 156.6 ± 8.0 and 148.0 ± 2.7 kJ/mol respectively, which agreed with 155.0 kJ/mol from the MALT database using protium instead of deutrium. As the enthalpies obtained from the observed gaseous vapor pressures are confirmed to be reasonable, we next evaluate the thermodynamic properties of Li_2TiO_3 and $Li_{2.12(2)}TiO_{3+y}$ in the following section.

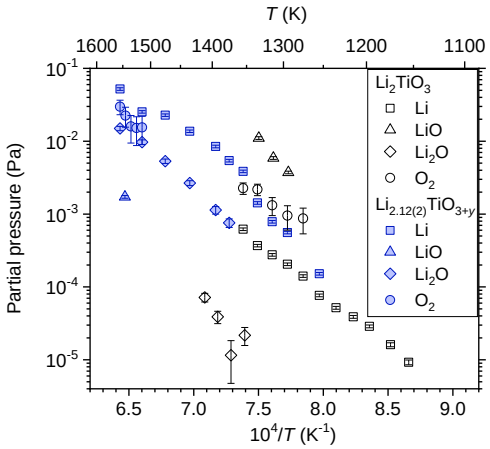

Figure 3. Vapor pressures from the stoichiometric Li_2TiO_3 and the hyper-stoichiometric $Li_{2.12}TiO_{3+y}$ pebbles in vacuum atmosphere.

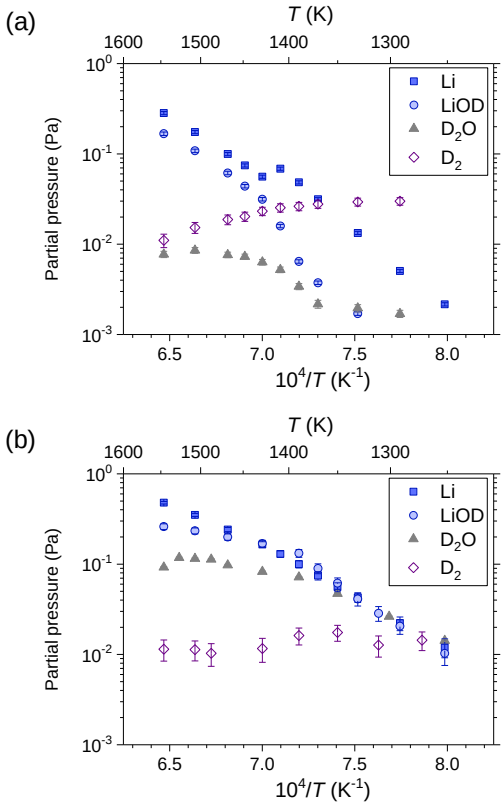

Figure 4. Vapor pressures from (a) the stoichiometric Li_2TiO_3 and (b) the hyper-stoichiometric $Li_{2.12}TiO_{3+y}$ pebbles measured in D_2 atmosphere.

3.2. Thermodynamic activities

Figure 5 displays Li activities in Li_2O, Li_2TiO_3, $Li_{2.12(2)}TiO_{3+y}$, and Li_4TiO_4 in the temperature range of 1155–1355 K. Li activities in the mixtures ($a_{Li,mixture}$) were directly obtained from the Li pressures from the sample and Li metal (Figure 5a). The vapor pressures of $Li_{(g)}$ from Li metal, Li_2O, Li_2TiO_3, and Li_4TiO_4 were taken from the literatures.[33,34,37,38] This direct approach, however, resulted in large discrepancies for the same compounds. For example, our data of a_{Li,Li_2TiO_3} had a poor agreement with the data of Li_2TiO_3 by Nakagawa *et al*.[33] Additionally, the Li activities in $Li_2O_{(s)}$ using the data by Kimura *et al*.[34] and Kudo *et al*.[37] were obviously inconsistent. This is explained by significant influence of oxygen partial pressures in the measurements. In principle, Li vaporization is enhanced under a reducing atmosphere and conversely suppressed under an oxidizing atmosphere by taking the equilibrium reactions in Eqs. (4) and (5) into account. Indeed, the measurement over $Li_2O_{(s)}$ under the low oxygen pressure (8.4×10^{-5} Pa at 1500 K) by Kimura *et al*. had a higher Li activity than the one obtained from the Kudo's data measured at 1.6×10^{-2} Pa (Figure 5a). The same was true for Li_2TiO_3; the previous study had approximately two orders of magnitude smaller O_2 partial pressure than our experiments, which resulted in approximately one order of magnitude larger p_{Li} than ours. On this basis, the direct approach is unsuitable for evaluating Li activities in the Li oxides due to the significant influence of oxygen concentrations.

To take the oxygen influence into account, $p_{Li,mixture}$ is converted into a function of equilibrium constant and oxygen pressure. The following reactions were considered for $Li_{(g)}$ vapor over $Li_2O_{(s)}$ and $Li_4TiO_{4(s)}$ in vacuum.

$$Li_2O_{(s)} \leftrightarrow 2Li_{(g)} + 0.5O_{2(g)} \quad (11)$$

$$Li_4TiO_{4(s)} \leftrightarrow 2Li_{(g)} + 0.5O_{2(g)} + Li_2TiO_{3(s)} \quad (12)$$

Given that activities in the pure substances equal to 1, equilibrium constants K in the Eqs. (4), (5), (11), and (12) are described by partial pressures of Li and O_2, namely.

$$K = \left(\frac{p_{Li,mixture}}{p_0} \right)^2 \left(\frac{p_{O_2,mixture}}{p_0} \right)^{0.5} \quad (13)$$

From Eqs. (2) and (13), Li activity in a mixture can be given as a function of temperature and oxygen pressure as follows:

$$a_{\mathrm{Li,mixture}} = \frac{p_{\mathrm{Li,mixture}}}{p_{\mathrm{Li,pure}}} \left(\frac{p_{\mathrm{D_2O,mixture}}}{K_9 p_{\mathrm{D_2,mixture}}} \right)^{0.5} \left(\frac{p_0}{p_{\mathrm{O_2,mixture}}} \right)^{0.25} \quad (14)$$

where p is partial pressure (Pa), p_0 is the standard pressure (101325 Pa), and K_9 is equilibrium constant of Eq. (9). The measured data of $p_{\mathrm{Li,mixture}}$, $p_{\mathrm{D_2}}$, and $p_{\mathrm{D_2O}}$ in D_2 atmosphere (Figure 4) were used, while K_9 was taken from the JANAF table.[31] Li activity in the Li oxides is described as an inverse function of fourth root of partial oxygen pressure. Here, Li activities under a reducing atmosphere ($p_{\mathrm{O_2}}/p_0 = 10^{-5}$) was considered because the oxygen concentrations in outlet gas in our previous long-term compatibility test with the hyper-stoichiometric sample (Li/Ti = 2.15 at mixing) were 10–30 ppm.[23] Figure 5b represent Li activities obtained using Eq. (14) and the equilibrium constants of K_4, K_5, K_{11}, and K_{12}. Unlike the direct approach (Figure 5a), the Li activity in the Li_2TiO_3 pebbles in this work showed an excellent agreement with the data by Nakagawa *et al,*[33] despite the large difference in the measured oxygen partial pressures. The Li activities in $Li_2O_{(s)}$ by the two groups agreed well too.[34,37] Therefore, we consider the indirect approach is valid for data measured in different oxygen concentrations. Noted that the obtained Li activity in Figure 5b were larger than the direct approach (Figure 5a) due to propagation of error in Eq. (13). As a result, Li activity in $Li_4TiO_{4(s)}$ was evaluated to be as high as that in $Li_2O_{(s)}$. All the Li activities showed similar gradients of temperature dependency, which allows extrapolations to lower temperature. The Li activity in $Li_{2.12(2)}TiO_{3+y}$ was approximately one order greater than that in Li_2TiO_3 and one order smaller order than those of Li_2O and Li_4TiO_4. This enhancement of Li activity in $Li_{2.12(2)}TiO_{3+y}$ could be explained by the accommodation of excess Li, especially in interstitial Li atoms weakly bonded with four surrounding oxygen atoms.[16]

The following reactions were considered for evaporation of $Li_2O_{(g)}$ over the Li-containing oxides.

$$Li_2TiO_{3(s)} \leftrightarrow Li_2O_{(g)} + TiO_{2(s)} \quad (15)$$

$$Li_{2+2x}TiO_{3+x(s)} \leftrightarrow Li_2O_{(g)} + xLi_2O_{(s)} + TiO_{2(s)} \quad (16)$$

$$Li_2O_{(s)} \leftrightarrow Li_2O_{(g)} \quad (17)$$

$$Li_4TiO_{4(s)} \leftrightarrow Li_2O_{(g)} + Li_2TiO_{3(s)} \quad (18)$$

Li_2O activities from the Li-containing compounds were directly obtained from the vapor pressures of $Li_2O_{(g)}$ from pure $Li_2O(s)$[37] and the mixtures using Eq. (2). This is because the $Li_2O_{(g)}$ reactions are independent from $O_{2(g)}$. Li_2O activities in Li_2O, Li_2TiO_3, $Li_{2.12(2)}TiO_{3+y}$, and Li_4TiO_4 are shown in Figure 6. The Li_2O activity in $Li_{2.12(2)}TiO_{3+y}$ was

evaluated to be one order of magnitude smaller than Li_4TiO_4 and greater than that in Li_2TiO_3. The activity analysis indicates the higher activities in $Li_{2.12}TiO_{3+y}$ than Li_2TiO_3, which results in enhanced Li loss from the hyper-stoichiometric pebbles. It should be noted that the results also show the enhanced release of oxygen from the hyper-stoichiometric pebbles as form of $O_{2(g)}$ and $Li_2O_{(g)}$. This is important because the corrosion layer on RAFM steels is formed by oxygen release from breeder materials and the growth is controlled by the diffusion.[23,27] The reported enhancement of the corrosion by the hyper-stoichiometric breeder material can be attributed enhanced oxygen release originating from the increases of the thermodynamic activities.

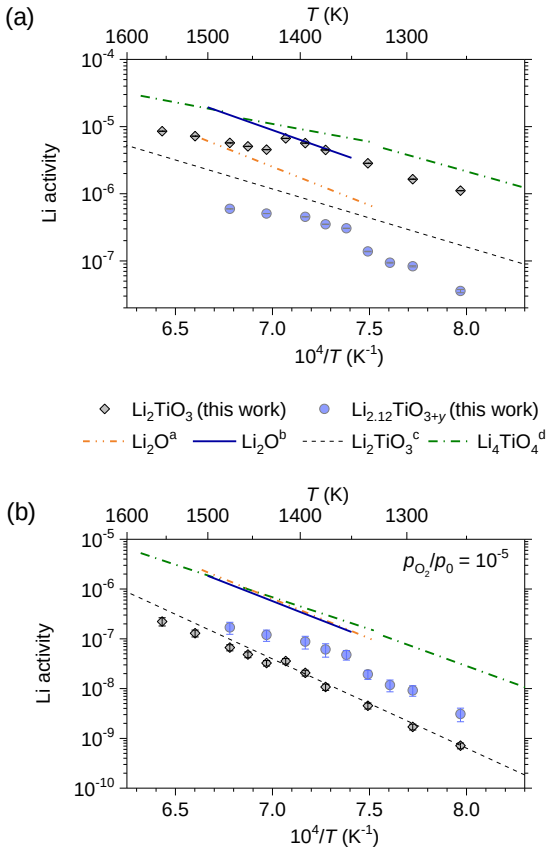

Figure 5. Li activities in Li_2O, Li_2TiO_3, $Li_{2.12}TiO_{3+y}$, and Li_4TiO_4 obtained (a) by the direct approach using Eq. (2) and (b) from the equilibrium constants using Eq. (14). In panel (b), partial pressure of oxygen was set to be $10^{-5} \times p_0$.

[a] Reference [34]
[b] Reference [37]
[c] Reference [33]
[d] Reference [38]

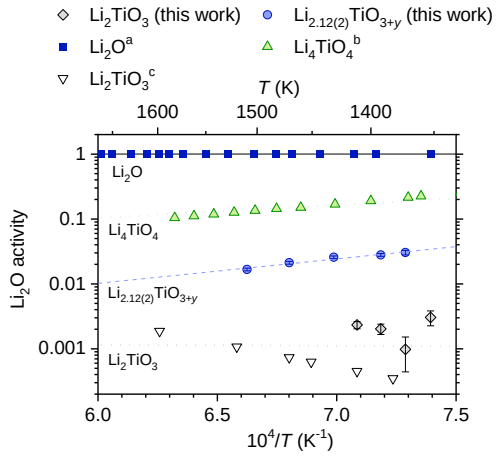

Figure 6. Li_2O activities in Li_2O, Li_2TiO_3, $Li_{2.12}TiO_{3+y}$, and Li_4TiO_4 directly obtained from partial pressures of $Li_2O_{(g)}$ and Eq. (2).

[a] Reference [37]
[b] Reference [38]
[c] Reference [33]

3.3. Evaluation of Li loss

In a fusion blanket, ceramic breeder pebbles will be used at elevated temperatures (maximum temperature: 1173 K) in a reducing atmosphere (sweep gas composition: He + 0.1 vol.% H_2). Hence, Li vapor pressures in the blanket environments were evaluated using the data obtained in D_2 atmosphere below the β-γ transformation temperature. The total pressure of Li-containing species $p_{\mathrm{Li}}^{\mathrm{total}}$ is defined to be $p_{\mathrm{Li}}^{\mathrm{total}} = p_{\mathrm{Li}} + p_{\mathrm{LiOD}}$. Based on the reactions in Eqs. (4) and (6), $p_{\mathrm{Li}}^{\mathrm{total}}$ from the Li_2TiO_3 pebbles is given from the following equation.

$$p_{\mathrm{Li}}^{\mathrm{total}} = \sqrt{p_0^2 p_{\mathrm{D_2}} K_4 K_8 / p_{\mathrm{D_2O}}} + \sqrt{K_6 p_0 p_{\mathrm{D_2O}}} \quad (19)$$

From Eqs. (5) and (7), $p_{\mathrm{Li}}^{\mathrm{total}}$ from the hyper-stoichiometric $Li_{2.12(2)}TiO_{3+y}$ pebbles is given as follows.

$$p_{\mathrm{Li}}^{\mathrm{total}} = \sqrt{p_0^2 p_{\mathrm{D_2}} K_5 K_8 / p_{\mathrm{D_2O}}} + \sqrt{K_7 p_0 p_{\mathrm{D_2O}}} \quad (20)$$

Based on the sweep gas composition, the partial pressure of deuterium gas was set to be $10^{-3} \times p_0$ (Pa). The limit of $p_{\mathrm{Li}}^{\mathrm{total}}$ in breeding blanket was set to be 0.01 Pa.[39] The total pressures of Li-containing species from the stoichiometric and hyper-stoichiometric pebbles at the partial pressure of moisture from 0.01 to 1000 Pa are shown in Figure 7. In Figure 7a, $p_{\mathrm{Li}}^{\mathrm{total}}$ from the stoichiometric pebbles were below the limit at T = 1073 K or lower temperatures. The total pressure at T = 1173 K exceeded the limit at a partial pressure of moisture greater than 36 Pa. On the contrary, $p_{\mathrm{Li}}^{\mathrm{total}}$ from the hyper-stoichiometric $Li_{2.12(2)}TiO_{3+y}$ pebbles showed the elevated pressures compared with the stoichiometric

pebbles (Figure 7b), in which the pressures at 973 and 1073 K exceeded the limit in some moisture concentrations. The results suggest that the moisture concentration in sweep gas should be kept in the range of 0.1–10 Pa to minimize the loss of Li from the hyper-stoichiometric pebbles. The total pressure from the hyper-stoichiometric pebbles at 1173 K was above the limit in any moisture concentrations between 0.1 and 1000 Pa. Yet, the results do not necessarily mean that total pressure in a blanket with the $Li_{2.12(2)}TiO_{3+y}$ pebbles is above the limit. This is because a breeder zone has temperature distribution and only the central part achieves very high temperature above 973 K. Li loss from the pebbles in a breeding zone with inhomogeneous temperature distribution was modeled as follows.

Presently, cylindrical and honeycomb-shaped breeding blanket are under study for demonstration fusion reactors.[40,41] Herein, total pressure of Li-containing species in a cylindrical blanket with ceramic breeder pebbles with water coolant was analyzed. The results of the analysis are shown in Figure 8. It was considered that temperatures in a cylindrical breeding zone with arbitrary radius and length are distributed from 623 to 1173 K (inset in Figure 8). The breeding zone was separated into 56 sections with temperature step of 10 K in the radius direction, in which the maximum and minimum temperatures were set to be 1173 K (innermost section 1) and 623 K (outermost section 56), respectively. The total pressure of Li-containing species in the breeding zone $p_{\mathrm{total,blanket}}$ was given as follows.

$$p_{\mathrm{total,blanket}} = \sum_{j=1}^{56} p_{\mathrm{Li}}^{\mathrm{total}}(T, p_{\mathrm{moisture}}) \left(\frac{V_j}{V} \right) \tag{21}$$

where V_j is the volume of section j (j = 1–56) and V is the total volume of the breeding zone. The volume fraction V_j/V is independent of radius and length, but dependent only on j. In Figure 8, the results showed the significant influence of environmental moisture concentration on the total pressure and the dominant vapor species. The contribution of $LiOH_{(g)}$ increased with moisture concentration and became the dominant gas species in a wet condition at p_{moisture} >10 Pa. The results showed that $p_{\mathrm{total,blanket}}$ became minimum values when p_{Li} and p_{LiOH} were equivalent. The total pressure in the breeding zone with the Li_2TiO_3 pebbles was below the limit at any moisture concentrations. In case of the hyper-stoichiometric $Li_{2.12}TiO_{3+y}$ pebbles, the pressure was at least one order of magnitude higher than that with the Li_2TiO_3 pebbles. The breeding zone with the hyper-stoichiometric pebbles was below the limit at most of moisture concentrations, but it exceeded the limit in humid conditions in $p_{\mathrm{moisture}} > 200$ Pa. Such a high humidity would not be achieved only by water release from the breeder pebbles, as the moisture concentration is one order of magnitude greater than the ones in the outlet gas in the previous experiments purging

the dry sweep gas of He + 0.1 vol.% H_2.[20,23] The results of the modeling show the insight into the role of moisture concentration in equilibrium regime, determining the optimum condition suppressing Li loss by vaporization. In a fusion blanket, humidity in a breeding zone may be increased by tritium production and substantial release of HTO gas from the pebbles, although the main form was not HTO but HT in the previous DT neutron irradiation test of the $Li_{2.13}TiO_{3+y}$ pebbles.[42] As a blanket environment is in a non-equilibrium regime, further investigations are needed to understand mass transfer properties and its interaction with tritium release from the breeder pebbles.

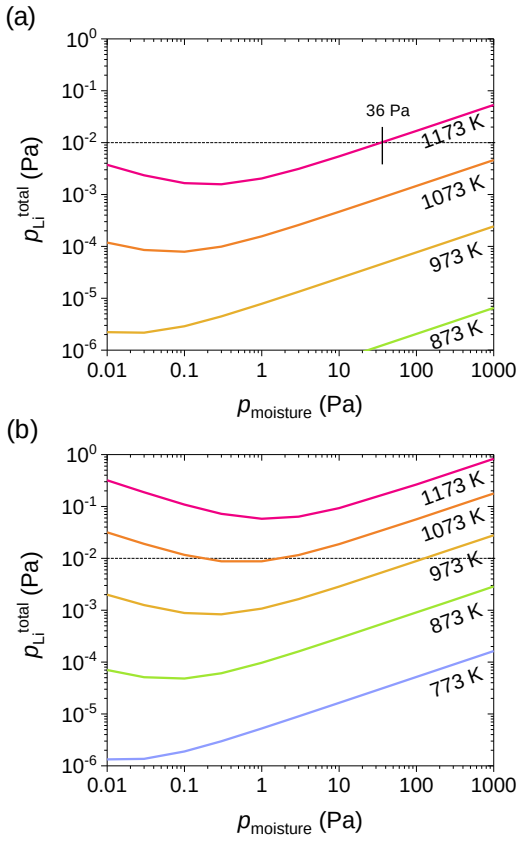

Figure 7. The dependency of p_{Li}^{total} on moisture concentration at various temperatures from (a) the stoichiometric and (b) the hyper-stoichiometric pebbles. Black horizontal line denotes the limit of p_{Li}^{total} = 0.01 Pa.

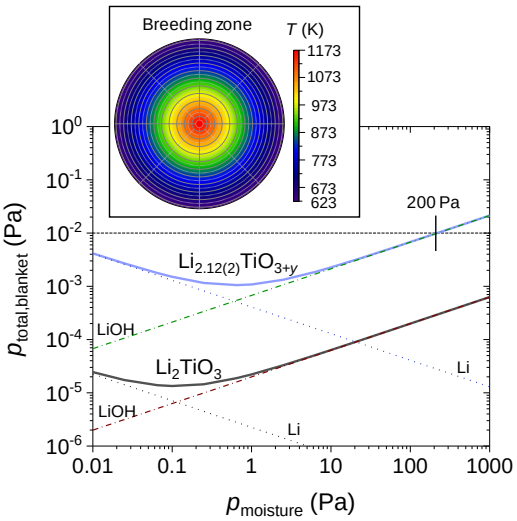

Figure 8. The effect of moisture concentration on the total pressure of Li-containing species in the breeding zone $p_{total,blanket}$, in which dotted and dash-dot lines denote contributions of $Li_{(g)}$ and $LiOH_{(g)}$ respectively. Horizontal broken line denotes the limit of 0.01 Pa. Inset shows the temperature distribution in cross section of the cylindrical blanket.

4. Conclusion

Thermodynamic properties of hyper-stoichiometric lithium metatitanate $Li_{2.12(2)}TiO_{3+y}$ and the vapor reactions over the pebbles have been evaluated by atmosphere controllable Knudsen cell mass spectrometry for the first time. By measuring the partial pressures over the breeder pebbles, the thermodynamic activities and the equilibrium constants of the vapor reactions were obtained. The thermodynamic activities of Li in the mixtures were indirectly obtained as functions of the equilibrium constant to include the influence of oxygen pressure and compared with the Li(–Ti)–O ceramics. The activities of Li and Li_2O of $Li_{2.12(2)}TiO_{3+y}$ were evaluated to be approximately one order of magnitude higher than those in Li_2TiO_3, suggesting enhanced releases of gas species containing Li and O. The total pressure of Li-containing species from the hyper-stoichiometric pebbles in the breeding zone with temperature distribution (623–1173 K) was below the limit at a partial pressure of moisture below 200 Pa. Li loss by vaporization over the hyper-stoichiometric pebbles can be minimized in the moisture partial pressure range of 1–10 Pa in which partial pressures of $Li_{(g)}$ and $LiOH_{(g)}$ are equivalent. The results demonstrated the importance of moisture concentration in the breeding zone as it has significantly impact on Li loss by vaporization, which, in turn, affects tritium breeding performance and corrosion behavior of reduced activation ferritic-martensitic structural steel.

Associate content

Supporting Information

The supporting information is available free of charge.

Ionization voltage curve, Calibration using Ag standard sample, temperature dependencies of vapor gas pressures in vacuum and D_2 (Figure S1–S2 and Tables S1–S2).

Author Information

Corresponding author

E-mail: k-mukai@iae.kyoto-u.ac.jp (K.M.)

ORCID

Keisuke Mukai: 0000-0001-8067-8732

Notes

The authors declare no competing financial interest.

Acknowledgement

This work was financially supported by JSPS Research Fellowship DC2 (24-5331) and JSPS Postdoctoral Fellowships for Research Abroad to KM. Tsuyoshi Hoshino is thanked for pebble fabrication and helpful discussions.

References

1 Knaster, J.; Moeslang, A.; Muroga, T. Materials research for fusion. *Nat. Phys*. **2016**, *12*, 424–434.

2 Lee, W. E.; Gilbert, M.; Murphy, S. T.; Grimes, R. W. Opportunities for advanced ceramics and composites in the nuclear sector. *J. Am. Ceram. Soc*. **2013**, *96* (7), 2005–2030.

3 Zmitko, M.; Vladimirov, P.; Knitter, R.; Kolb, M.; Leys, O.; Heuser, J.; Schneider, H. C.; Rolli, R.; Chakin, V.; Pupeschi, S.; *et al*. Development and qualification of functional materials for the European HCPB TBM. *Fusion Eng. Des.* **2018**, *136*, 1376–1385.

4 Kawamura, Y.; Tanigawa, H.; Hirose, T.; Enoeda, M.; Sato, S.; Ochiai, K.; Konno, C.; Edao, Y.; Hayashi, T.; Hoshino, T.; Nakamichi, M. Progress of R&D on water cooled ceramic breeder for ITER test blanket system and DEMO. *Fusion Eng. Des.* **2016**, *109*, 1637–1643.

5 Wang, S.; Cao, Q.; Wu, X.; Wang, X.; Zhang, G.; Feng, K. Updated conceptual design of helium cooling ceramic blanket for HCCB-DEMO. *Fusion Eng. Des*. **2016**, *112*, 148–155.

6 Hernández, F. A.; Arbeiter, F.; Boccaccini, L. V.; Bubelis, E.; Chakin, V. P.; Cristescu, I.; Ghidersa, B. E.; González, M.; Hering, W.; Hernández, T.; Jin, X. Z. Overview of the HCPB research activities in EUROfusion. *IEEE Trans. Plasma Sci.* **2018**, *46*, 2247–2261.

7 Leys, O.; Kolb, M.; Pucci, A.; Knitter, R. Study of lithium germanate additions to advanced ceramic breeder pebbles. *J. Nucl. Mater*. **2019**, *518*, 234–240.

8 Konishi, S.; Enoeda, M.; Nakamichi, M.; Hoshino, T.; Ying, A.; Sharafat, S.; Smolentsev, S. Functional materials for breeding blankets—status and developments. *Nucl. Fusion* **2017**, *57*, 092014.

9 Tanigawa, H.; Hoshino, T.; Kawamura, Y.; Nakamichi, M.; Ochiai, K.; Akiba, M.; Ando, M.; Enoeda, M.; Ezato, K.; Hayashi, K.; Hirose, T. R&D of a Li_2TiO_3 pebble bed for a test blanket module in JAEA. *Nucl. Fusion* **2009**, *49*, 055021.

10 Kataoka, K.; Takahashi, Y.; Kijima, N.; Nagai, H.; Akimoto, J.; Idemoto, Y.; Ohshima, K. I. Crystal growth and structure refinement of monoclinic Li_2TiO_3. *Mater*. *Res*. *Bull*. **2009**, *44*, 168–172.

11 Azuma, K.; Dover, C.; Grinter, D. C.; Grau-Crespo, R.; Almora-Barrios, N.; Thornton, G.; Oda, T.; Tanaka, S. Scanning tunneling microscopy and molecular dynamics study of the Li_2TiO_3 (001) surface. *J. Phys*. *Chem*. *C* **2013**, *117*, 5126–5131.

12 Kleykamp, H. Phase equilibria in the Li–Ti–O system and physical properties of Li_2TiO_3. *Fusion Eng. Des.* **2002**, *61***,** 361–366.

13 Vijayakumar, M.; Kerisit, S.; Yang, Z.; Graff, G. L.; Liu, J.; Sears, J. A.; Burton, S. D.; Rosso, K. M.; Hu, J. Combined ^{6,7}Li NMR and molecular dynamics study of Li diffusion in Li_2TiO_3. *J. Phys*. *Chem*. *C* **2009**, *113*, 20108–20116.

14 Murphy, S. T.; Hine, N. D. Point defects and non-stoichiometry in Li_2TiO_3. *Chem*. *Mater.* **2014**, *26*, 1629–1638.

15 Murphy, S. T. Tritium solubility in Li_2TiO_3 from first-principles simulations. *J. Phys*. *Chem*. *C* **2014**, *118*, 29525–29532.

16 Mukai, K.; Yashima, M.; Hibino, K.; Terai, T. Experimental visualization of interstitialcy diffusion of Li ion in *β*-Li_2TiO_3. *ACS Appl*. *Energy Mater*. **2019**, *2*, 5481–5489.

17 Kobayashi, M.; Kawasaki, K.; Fujishima, T.; Miyahara, Y.; Oya, Y.; Okuno, K. Release kinetics of tritium generated in lithium-enriched $Li_{2+x}TiO_3$ by thermal neutron irradiation. *Fusion Eng. Des.* **2012**, *87*, 471–475.

18 Hoshino, T. Optimization of sintering conditions of advanced tritium breeder pebbles fabricated by the emulsion method. *Fusion Eng. Des.* **2015**, *98*, 1788–1791.

19 Hara, M.; Togashi, Y.; Matsuyama, M.; Oya, Y.; Okuno, K. Crystal structure change of $Li_{2+x}TiO_{3+y}$ tritium breeder under moist air. *J. Nucl. Mater.* **2010**, *404*, 217–221.

20 Shimozori, M.; Katayama, K.; Hoshino, T.; Ushida, H.; Yamamoto, R.; Fukada, S. Water vapor concentration dependence and temperature dependence of Li mass loss from Li_2TiO_3 with excess Li and Li_4SiO_4. *Fusion Eng*. *Des*. **2015**, *98*, 1808–1811.

21 Mukai, K.; Sasaki, K.; Terai, T.; Suzuki, A.; Hoshino, T. Vaporization property and crystal structure of lithium metatitanate with excess Li. *J. Nucl. Mater.* **2013**, *442*, S447–S450.

22 Cho, S.; Park, Y. H.; Chun, Y. B.; Min, K. M.; Ahn, M. Y.; Park, S. C.; Lee, Y. Chemical compatibility between ARAA alloy and lithium meta-titanate breeder material. *Fusion Eng. Des.* **2017**, *124*, 1052–1058.

23 Mukai, K.; Sanchez, F.; Hoshino, T.; Knitter, R. Corrosion characteristics of reduced activation ferritic-martensitic steel EUROFER by Li_2TiO_3 with excess Li. *Nucl. Mater. Energy* **2018**, *15*, 190–194.

24 Hernández, T.; Gázquez, M. C.; Sánchez, F. J.; Malo, M. Corrosion mechanisms of Eurofer produced by lithium ceramics under fusion relevant conditions. *Nucl. Mater. Energy* **2018**, *15***,** 110–114.

25 Sonak, S.; Jain, U.; Haldar, R.; Kumar, S. Chemical compatibility study of lithium titanate with Indian reduced activation ferritic martensitic steel. *Fusion Eng. Des.* **2015**, *100*, 507–512.

26 Mukai, K.; Gonzalez, M.; Knitter, R. Effect of moisture in sweep gas on chemical compatibility between ceramic breeder and EUROFER97. *Fusion Eng. Des*. **2017**, *125*, 154–159.

27 Oishi, K.; Inoue, S.; Terai, T. In Proceedings of the 20th International Workshop on Ceramic Breeder Blanket Interactions (CBBI-20), KIT, Germany, Sept 18–20, 2019; Knitter, R. Ed.; 79–87. DOI: 10.5445/IR/1000100675

28 Yamawaki, M.; Suzuki, A.; Yasumoto, M.; Yamaguchi, K. Sweep gas chemistry effect on lithium transport from ceramic breeder blanket materials. *J. Nucl*. *Mater*. **1997**, *247*, 11–16.

29 Mann, J. B. In *Recent Developments in Mass Spectrometry*, Proceedings of the International Conference on Mass

Spectrometry, Kyoto, Japan; Ogata, K., Hayakawa, T., Eds.; University of Tokyo: Tokyo, 1970; 814–819.

30 Kordis, J.; Gingerich, K. A. Mass spectroscopic investigation of the equilibrium dissociation of gaseous Sb_2, Sb_3, Sb_4, SbP, SbP_3, and P_2. *J. Chem. Phys.* **1973**, *58*, 5141–5149.

31 Chase, M. W.; Davies, C. A.; Downey, J. R. Frurip, D. J.; McDonald, R. A.; Syverud, A. N. JANAF thermochemical tables. *Phys. Chem. Ref. Data Suppl.* **1985**, *14*, 1.

32 Alcock, C. B.; Itkin, V. P.; Horrigan, M. K. Vapour pressure equations for the metallic elements: 298–2500 K. *Can. Metall. Quart.* **1984**, *23*, 309–313.

33 Nakagawa, H.; Asano, M.; Kubo, K. Mass spectrometric investigation of the vaporization of Li_2TiO_3 (s). *J. Nucl. Mater.* **1982**, *110*, 158–163.

34 Kimura, H.; Asano, M.; Kubo, K. Thermochemical study of the vaporization of Li_2O (c) by mass spectrometric Knudsen effusion method. *J. Nucl. Mater.* **1980**, *92*, 221–228.

35 Yokokawa, H.; Yamauchi, S.; Matsumoto, T. Thermodynamic database MALT for windows with gem and CHD. *Calphad* **2002**, *26*, 155–166.

36 Hicks, W. T. Evaluation of vapor pressure data for mercury, lithium, sodium, and potassium. *J. Chem. Phys.* **1963**, *38*, 1873–1880.

37 Kudo, H.; Wu, C. H.; Ihle, H. R. Mass-spectrometric study of the vaporization of Li_2O (s) and thermochemistry of gaseous LiO, Li_2O, Li_3O, and Li_2O_2. *J. Nucl. Mater.* **1978**, *78*, 380–389.

38 Asano, M.; Nakagawa, H. Thermochemical study of vaporization of Li_4TiO_4 by a mass spectrometric Knudsen effusion method. *J. Nucl. Mater.* **1988**, *160*, 172–177.

39 Ihle, H. R.; Penzhorn, R. D.; Schuster, P. The thermochemistry of lithium silicates in view of their use as breeder materials. *Fusion Eng. Des.* **1989**, *8*, 393–397.

40 Tanigawa, H.; Gwon, H.; Hirose, T.; Kawamura, Y.; Ejiri, M.; Watanabe, K.; Asano, S.; Kokami, T.; Oda, Y. Cylindrical breeding blankets for fusion reactors. *Fusion Eng. Des.* **2018**, *36*, 1221–1225.

41 Tobita, K.; Hiwatari, R.; Sakamoto, Y.; Someya, Y.; Asakura, N.; Utoh, H.; Miyoshi, Y.; Tokunaga, S.; Homma, Y.; Kakudate, S.; Nakajima, N. Japan's efforts to develop the concept of JA DEMO during the past decade. *Fusion Sci. Technol.* **2019**, *75*, 372–383.

42 Hoshino, T.; Edao, Y.; Kawamura, Y.; Ochiai, K.; Pebble fabrication and tritium release properties of an advanced tritium breeder. *Fusion Eng. Des.* **2016**, *109*, 1114–1118.